THE ASTROPHYSICAL JOURNAL, 356:534–543, 1990 June 20

INFRARED AND RADIO MEASUREMENTS OF THE DENSITY STRUCTURE OF COMPACT H II REGIONS

S. T. MEGEATH, T. HERTER, G. E. GULL, AND J. R. HOUCK
Center for Radiophysics and Space Research, Cornell University
Received 1989 August 10; accepted 1989 December 22

ABSTRACT

The density structure of compact H II regions is studied by comparing the ratio of the [S III] 33.47 μm and 18.71 μm emission lines and 5 GHz continuum maps. Electron densities are computed for DR 22, G29.9−0.0, G75.84+0.4, M8, M42, S158, W3, and W33. For DR 22, M42, and W3, the electron densities determined from the infrared data are consistent with those derived from radio observations. The densities for S158 and M8 are quite low, implying that the S III emission is dominated by the diffuse ionized gas observed in the radio continuum. For G29.9−0.0, G75.84+0.4, and W33, the S III data give higher densities than predicted from radio observations. This implies that either these nebulae are filled with dense clumps of ionized gas which are not resolved in the radio maps, or that the S III zone is confined to the small, dense cores found in the radio maps of all three nebulae. Since the dynamical lifetime of dense, fully ionized clumps is short, it is likely that the S III zones in these regions are confined to the dense cores of the nebula. This is contrary to the predictions of current models of the ionization structure of H II regions. Several possible inadequacies of current models are discussed, and the effects of uncertainties in the ionic and density structure on abundance estimates in H II regions are investigated.

Subject headings: infrared: spectra — nebulae: H II regions

I. INTRODUCTION

Compact H II regions are an intermediate stage in the evolution of the ionized gas surrounding O and B stars. By definition, they range from 0.1–1.0 pc in diameter and have typical electron densities greater than 1000 cm^{-3}. The initial stage of H II region evolution occurs immediately after one or more stars begin nuclear burning and an ionization front moves outward into the molecular cloud. This stage lasts less than 1000 yr, ending as the region reaches a state of Strömgren equilibrium. The star is still buried within its natal environment and is not visible optically. The material surrounding the star is very dense; hence, the *ultracompact* H II region, which is small and optically thick at radio wavelengths, is difficult to detect (see Israel, Habing, and de Jong 1973). The rapid ionization and heating of the gas creates a large pressure differential between the ionized gas and the molecular cloud, producing a stage of rapid dynamical expansion. The density of the region quickly decreases, and a *compact* H II region forms. The large emission measure and intermediate size of compact H II regions allows them to be readily detected in the radio. Given an expansion speed close to the thermal sound speed, $\sim$10 km s^{-1}, on a time scale of $\sim 10^4$ yr the nebular size increases, the gas density drops, and the nebula moves through several stages to become a *diffuse* or *giant* H II region (see Habing and Israel 1979).

The relative youth of compact H II regions suggests that they may contain information on the initial star-forming environment. However, the rapid evolution of these regions may quickly alter the initial environment. For example, a nonuniform expansion can drastically change the density structure of the ionized gas. The rapid evolution of these regions also influences the surrounding molecular cloud and may trigger further star formation in the adjacent gas (see Klein, Sandford, and Whitaker 1983; Sandford, Whitaker, and Klein 1984). A better understanding of the electron density structure in compact H II regions should give insight into star formation and the evolution of star-forming regions.

Compact H II regions also offer an excellent means for studying galactic structure, since they can be detected throughout the galaxy at infrared and radio wavelengths. Many ions in these regions have strong emission lines in the infrared that can be used to estimate ionic and elemental abundances (see Herter *et al.* 1981, 1982*a*; Pipher *et al.* 1984; Lester *et al.* 1987; Rubin *et al.* 1988). However, to determine the ionic abundances, we must first understand the density structure of these regions, since the volume emissivities of the lines depend on the electron density.

Radio continuum observations are the most commonly used methods for determining the electron density in compact H II regions. The radio continuum flux density is a measure of the free-free emission of a nebula. Given a fully ionized cloud of hydrogen which is optically thin at wavelength ν, the total power per unit frequency due to free-free emission is proportional to the square of the electron density integrated over the volume of the cloud. The electron density for an H II region is calculated from the measured radio flux density by the equation

$$n_e^2 = \frac{1.06 \times 10^4 S_\nu(\mathrm{Jy}) D^2(\mathrm{kpc})}{V(\mathrm{pc}^3)} \times \left(\frac{\nu}{5\ \mathrm{GHz}}\right)^{0.1} \left(\frac{T_e}{7500\ \mathrm{K}}\right)^{0.35} \mathrm{cm}^{-6}, \quad (1)$$

where S_ν is the observed flux density, V is the volume of the source, T_e is the electron temperature of the emitting gas, and D is the distance to the region. The density determined from this equation has the advantage of being unaffected by interstellar extinction and only weakly dependent on temperature. The disadvantages of this technique are that it requires an estimate of the distance and volume of the emission region and that it is

an average over the inhomogeneities in the beam. The result of this method is an rms electron density globally averaged over the nebula.

Ionic line ratio measurements are another method for determining the electron density in compact H II regions. This technique has the advantage of being independent of the distance and volume of the emission region. Optical S II and O II line ratios have been used to measure the density in unobscured regions such as M42 (see Osterbrock 1974). The disadvantage of these lines is that that they are weighted toward regions of high temperature and may not sample the region uniformly. Furthermore, differential extinction can cause the observed emission to be weighted toward less obscured parts of the nebulae. Most recently, infrared line ratios from S III and O III have been used to determine densities in many H II regions (see Herter *et al.* 1982*b*; Melnick, Gull, and Harwit 1979; Lester *et al.* 1987; Rubin *et al.* 1988). In particular, the [S III] 18.71 μm and 33.47 μm line pair provides an excellent measure of electron density in compact H II regions. This line ratio is insensitive to temperature, quite sensitive to densities in the 1000–10,000 cm^{-3} range, and easily detected in optically obscured H II regions.

In contrast to the density derived from the radio continuum measurements, the [S III] 33.47 μm to 18.71 μm line ratio gives a local measurement of the density. Ideally, this measurement reflects the density of the electron gas surrounding the emitting S III ions, and it is independent of the volume and distance of the region. In reality, this measurement is a complicated average of the different densities found in the S III zone. For a qualitative understanding of this average, picture a compact H II region as composed of many different components each with a different density. The total 18.71 μm or 33.47 μm flux is the sum of the fluxes for each component,

$$F_{\mathrm{S\,III}} = \frac{x_i}{D^2} \sum_{k=1}^{N} X^k_{\mathrm{S\,III}} n_k{}^2 V_k (j_k/n_i n_e) , \qquad (2)$$

where $F_{\mathrm{S\,III}}$ is the line flux, N is the number of components, $j_k/n_e n_i$ is the emission coefficient per ion per electron of component k, V_k is the volume of component k, n_k is the electron density of component k, $X^k_{\mathrm{S\,III}}$ is the ratio of S III to sulfur in the kth component, x_i is the abundance ratio of sulfur to hydrogen, and D is the distance to the nebulae. The emission coefficient is approximately constant for densities well below the critical density. In this regime, the greater the volume and density of a component, the more it is represented by the [S III] emission. For densities much greater than the critical density, the emission coefficient is inversely proportional to the density. Thus, very dense components will not be well represented as compared to lower density components with equivalent values of $n_e^2 V$. This differs from the radio emission from the same volume for which $j_k/n_i n_e$ is independent of density. Thus, the radio density is not weighted toward regions of lower density. The combination of these effects can cause the densities determined from line ratio measurements and the rms densities determined from radio flux densities to be different.

Differences between the densities derived from atomic line ratios and radio continuum flux densities may reflect small-scale structure in the ionized gas. In particular, clumping of the gas may result in line ratio–derived densities much higher than the rms value. This is a model put forward to explain optical forbidden line observations of the Orion Nebula (see Osterbrock and Flathers 1959) and earlier S III measurements of the electron density in several H II regions (see Herter *et al.* 1982*b*). The usual picture is of high-density clumps located within a more diffuse gas. In this model, the S III line emission is dominated by the emission from the clumps (i.e., the clumps have a substantially larger $n_e^2 V$) and the S III density, which is a local measure of the gas density, reflects the density of the clumps. In comparison, radio measurements of the density average over the clumps and diffuse gas and the total volume is overestimated, giving a density lower than the density of the clumps. The S III density would then be higher than the radio density.

In this paper, we present a survey of the S III line ratios in compact H II regions and use these data to determine electron densities for the ionized gas. An earlier study found that in some H II regions, S III density estimates are much greater than those derived from the radio continuum measurements (Herter *et al.* 1982*b*). However, recently improved electron collision strengths lead to significant changes in these early S III results. The current study computes revised electron densities for the H II regions measured by Herter *et al.* (1982*b*) and provides S III density estimates for a larger sample of nebulae. We also present new radio continuum maps for three H II regions, DR 22, G75.84+0.4, and G29.9−0.0. These maps are used to make a more detailed examination of the density structure of several H II regions. Models constructed from these maps are compared with our S III data to examine whether the density structure of these regions is dominated by global density gradients or small, unobserved clumps of gas.

II. OBSERVATIONS

Observations of the [S III] 18.71 μm and 33.47 μm lines were made with the Cornell dual-grating spectrometer (Houck and Gull 1982) using the 91 cm telescope of the NASA Kuiper Airborne Observatory (KAO). The average altitude of the observations was 12.8 km. This project was one of several projects executed on 16 different flights between 1982 and 1987. For the 18.71 μm measurements, the spectrometer uses three Si:Sb detectors, each with an in-flight noise equivalent flux density (NEFD) of 6×10^{-18} W $Hz^{-1/2}$ cm^{-2}. The resolution at 18.71 μm was 0.034 μm. For the first nine flights, the 33.47 μm measurements were made with three Ge:Ga detectors each with an in-flight NEFD of 4×10^{-17} W $Hz^{-1/2}$ cm^{-2} and a resolution of 0.070 μm. After the ninth flight, these detectors were replaced by three Ge:Be detectors, each with an in-flight NEFD of 1.2×10^{-17} W $Hz^{-1/2}$ cm^{-2} and a resolution of 0.060 μm. Table 1 gives a log of the objects and positions observed.

The beam size for the first nine flights was 26″; subsequently, the beam size was changed to 28″. Spatial chopping was done at a frequency of 26 Hz, with beam switching occurring every 10 s. The chop direction and amplitude were chosen for each object to avoid chopping between two positions in the source. Since the sources are generally not visible optically, offset guiding was used. For most of these sources, an infrared peak was determined from measurements at several positions in the source, and the beam was centered on the peak position. Table 2 lists the measured line fluxes for the 18.7 μm and 33.5 μm lines. For W3 and M42, some limited mapping in the S III lines was performed. The infrared beam positions are indicated on radio maps of M42 and W3 in Figures 1 and 2. Since the observations were carried during different times of the year, a variety of calibrators were used. The calibrators were α Ori, IRC+10420, Jupiter, Mars, and the Moon.

TABLE 1

SOURCE POSITIONS

Source	α_{1950}	σ_{1950}	Comment	References[a]	θ_B[b]
DR 22	$20^h37^m37^s$	41°09′22″	Radio Peak	Fig. 3	28
G1.1−0.1	17 45 32.2	−28 00 42	Radio Peak	1	28
G8.1+0.2	18 00 00.9	−21 48 17	Radio Peak	2	28
G25.4−0.2	18 35 25.0	−06 48 25	Radio Peak	2	28
G29.9−0.0	18 43 27	−02 42 37	Radio Peak	Fig. 4	28
G75.84+0.4	20 19 47	37 21 30	Radio Peak	3	26
K3-50 A	19 59 50	33 24 20	Radio Peak	4	28
K3-50 B	19 59 52	33 24 40	Radio Peak	4	28
K3-50 C1	19 59 58	33 25 51	Radio Peak	4	28
K3-50 C2	19 59 60	33 25 51	Radio Peak	4	28
K3-50 D	19 59 52	33 23 20	Radio Peak	4	28
M8	18 00 37	−24 23 00	Radio Peak	5	26
M42	...	...	See Fig. 1		26
S158A	23 11 22	61 13 50	IRS 5	6	26
W3	...	...	See Fig. 2		28
W33	18 11 18	−17 56 38	IRS 3	7	28
W43	18 44 59	−01 58 57	E.Rad. Pk	8	26

[a] REFERENCES.—(1) Downes *et al.* 1978; (2) Woodward, Helfer, and Pipher 1985; (3) Matthews *et al.* 1973; (4) Israel 1976; (5) Woodward *et al.* 1986; (6) Wynn-Williams, Becklin, and Neugebauer 1973; (7) Dyck and Simon 1977; (8) Pipher, Grasdalen, and Soifer 1974.

[b] Beam diameter for S III measurements.

Radio continuum observations of DR 22, G29.9−0.0, and G75.84+0.4 were carried out using the NRAO Very Large Array (VLA).[1] Figures 3, 4, and 5 show the radio maps obtained for these three regions, respectively. These sources were among seven objects observed over a 12 hr period. The VLA was in the A-configuration with 18 antennae functioning. The sources were observed in the 4.885 GHz band with a 50 MHz bandwidth. The observation of each source was divided into 10 minute integrations which were spread throughout the 12 hr observing period for maximum UV coverage. Approximately 80 minutes of total integration time was spent on each source. To compensate for phase and amplitude variations due to atmospheric and instrumental effects, calibrator sources were observed prior to each integration. The primary flux calibrator was 3C 286. The phase calibrators were 2005+403 for DR 22 and G75.84+0.4 and 1821+107 for G29.9−0.0.

[1] The National Radio Astronomical Observatory is operated by Associated Universities, Inc., under cooperative agreement with the National Science Foundation.

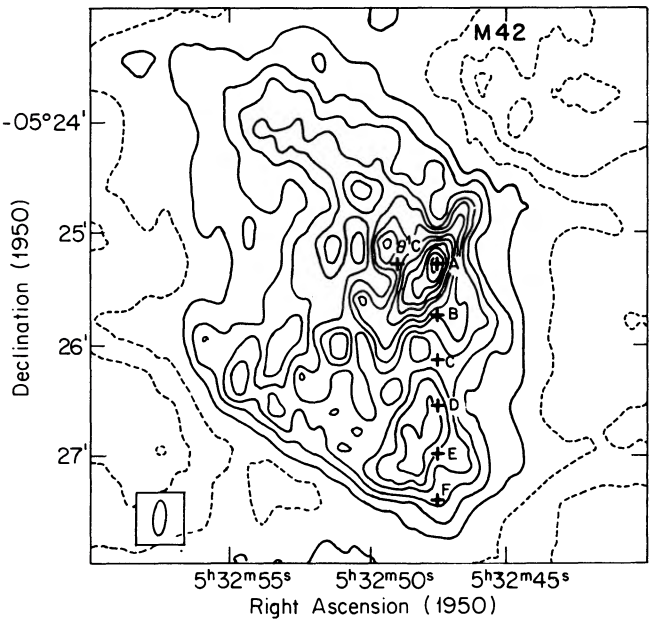

FIG. 1.—Five gigahertz continuum radio map of M42 from Martin and Gull (1976). The map has been cleaned and has a resolution of 7″ × 20″ in R.A. and declination, respectively. The total flux of the region at 5 GHz is 134 Jy. The cross to the left gives the position of θ^1C. The crosses to the right give the beam positions at which the S III measurement were made.

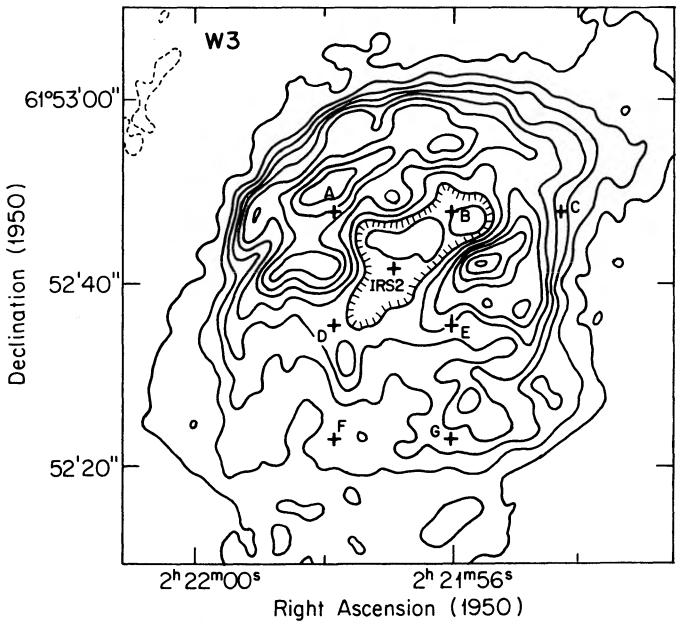

FIG. 2.—Five gigahertz continuum radio map of W3 from Harris and Wynn-Williams (1976). The synthesized half-power beamwidth is 2″.0 × 2″.3 in the R.A. and declination, respectively. The total flux of the region at 5 GHz is 33±4 Jy. The crosses give the position of the S III measurements.

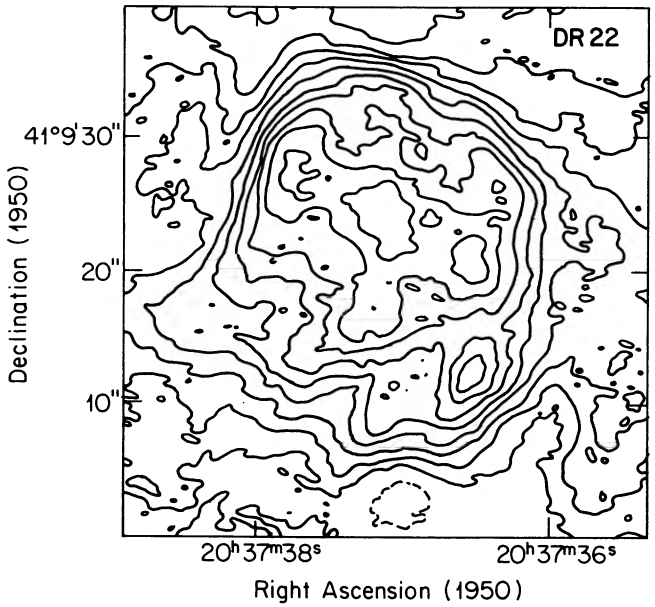

FIG. 3.—Five gigahertz continuum radio map of DR 22 made with the VLA in the A-configuration. This map in uncleaned; the low-intensity emission to the east and west is the effect of sidelobes. The beam size is 3".5 × 1".9 in R.A. and declination, respectively. The contour levels are separated by 10% of the peak flux, starting with the 10% contour. The total flux of the region at 10.5 GHz is 3.2 Jy (Felli, Tofani, and D'Addario 1974).

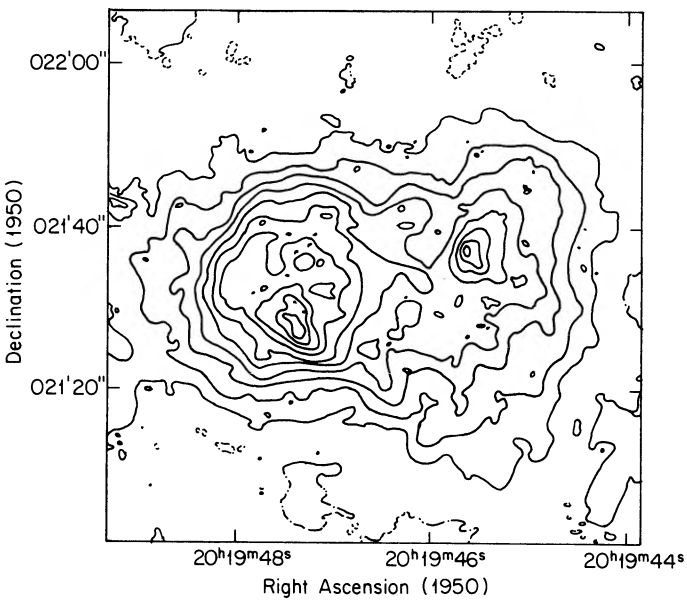

FIG. 5.—Five gigahertz continuum radio map of G75.84+0.4, made with the VLA in the A-configuration. As in the case of DR 22, this map is uncleaned. The beam size is 4" × 1".9 in R.A. and declination, respectively. The contour levels are separated by 10% of the peak flux, starting with the 10% contour. The total flux of the region at 10.7 GHz is 7.8 ± 0.8 Jy (Matthews *et al.* 1973).

III. ELECTRON DENSITIES IN COMPACT H II REGIONS

The [S III] 18.71 μm and 33.47 μm forbidden lines result from spontaneous emission from the $^3P_2$ and $^3P_1$ fine-structure levels of the ground state of the ion. The levels are excited through electron collisions, and the population of the levels are determined by the balance between collisional excitation and radiative and collisional de-excitation. Since the S III lines are always optically thin, simulated processes do not affect the level populations. The volume emissivity of the lines is computed as a function of density and temperature by solving the rate equations of a five-level model of the S III ion (see Osterbrock 1974) using the updated collision strengths of Mendoza (1983). Figure 6 shows the calculated variation in the S III line ratio as a function of density and temperature.

Because the observed H II regions are associated with molecular clouds and may be quite distant, a significant extinction correction must be applied for some of the nebulae. Adopting the extinction curve of Herter *et al.* (1982*b*), the extinctions at

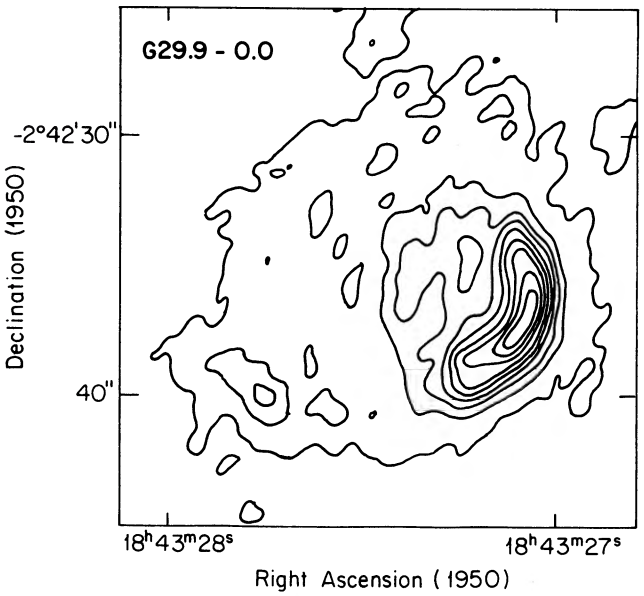

FIG. 4.—Five gigahertz continuum radio map of G29.9−0.0 made with the VLA in the A-configuration. This map has been cleaned. The beam size is 2".9 × 4".6 in R.A. and declination, respectively. The contour levels are separated by 10% of the peak flux, starting with the 10% contour. The total flux of the region at 10.5 GHz is 2.9 Jy (Felli, Tofani, and D'Addario 1974).

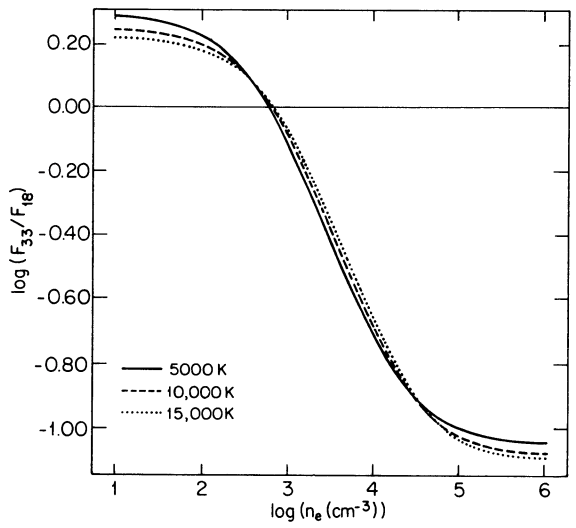

FIG. 6.—log (F_{33}/F_{18}) for electron densities between 100 and 10,000 cm^{-3}. The curve is shown for three different electron temperatures: 15,000 K, 10,000 K, and 5000 K. Typical electron temperatures are in the range 6000–9000 K for compact H II regions.

TABLE 2

S III DATA

Source	$F_\lambda(18.7)^a$	$F_\lambda(33.5)^a$	$\tau_{9.7}$	$F_{33}/F_{18}{}^b$
DR 22	16.6 ± 1.6	12.8 ± 3.4	2.2 ± 0.3	0.31 ± 0.09
G1.1−0.1	31.2 ± 1.2	35.7 ± 4.4	...	...
G8.1+0.2	19.5 ± 2.2	26.4 ± 2.5	...	...
G25.4−0.2	4.8 ± 0.9	12.9 ± 1.9	...	...
G29.9−0.0	38.2 ± 3.9	21.6 ± 3.8	2.5 ± 0.2	0.20 ± 0.04
G75.84+0.4	30.4 ± 4.7	14.9 ± 2.6	2.1 ± 0.1	0.20 ± 0.05
K3-50 A	9.0 ± 1.2	7.0 ± 1.1	...	...
K3-50 B	18.5 ± 2.0	22.5 ± 2.4	...	...
K3-50 C1	2.8 ± 0.8	7.4 ± 1.1	...	...
K3-50 C2	6.1 ± 1.2	8.5 ± 1.4	...	...
K3-50 D	16.9 ± 2.0	19.8 ± 2.6	...	...
M8	26.0 ± 2.9	30.5 ± 4.7	0	1.17 ± 0.22
M42 θ^1C	60.1 ± 8.2	20.7 ± 3.4	0	0.34 ± 0.07
S158A	14.0 ± 1.6	25.6 ± 4.5	0.30 ± 0.03	1.62 ± 0.34
W3 A	43.6 ± 5.8	30.4 ± 4.9	1.9 ± 0.3	0.32 ± 0.08
W33	12.6 ± 1.5	15.2 ± 2.7	4.3 ± 0.4	0.20 ± 0.05
W43	16.6 ± 1.9	40.7 ± 5.6	...	...

[a] S III line flux in units of 10^{-18} W cm^{-2}.
[b] Extinction corrected line ratio.

18.71 μm and 33.47 μm are $0.62\tau_{9.7}$ and $0.20\tau_{9.7}$, respectively, where $\tau_{9.7}$ is the optical depth in the "silicate" feature at 9.7 μm due to intervening dust absorption. Table 2 lists $\tau_{9.7}$ for the nine of the 13 observed H II regions which have extinction data. The corrected line ratios for S III are also listed in Table 2.

The electron density of a nebula is determined by comparing the corrected S III line ratio with the curve in Figure 6. We assumed a temperature of 8000 K, which is accurate to 15% for most compact H II regions. Figure 6 shows that the 33.47 μm to 18.71 μm line ratio is not significantly altered by temperature changes of this magnitude. To express the uncertainty in density, we give the electron density for a line ratio 1 σ greater and less than the mean line ratio. The resulting densities are listed in Table 3.

IV. COMPARISON OF S III AND RADIO OBSERVATIONS

In the following section, we compare the S III densities to densities derived from radio continuum observations of the nebula. From this comparison, we can learn whether the S III results are consistent with the density structure observed in high-resolution radio maps, or if further density structure such as clumping is needed to explain the results.

TABLE 3

ELECTRON DENSITIES AND ABUNDANCES

Source	S III Density (cm^{-3})[a]	S III/H[b]
DR 22	4800 (9000; 3100)	8.3×10^{-6}
G29.9−0.0	10000 (15800; 7100)	3.3×10^{-5}
G75.84+0.4	9700 (16300; 6600)	1.7×10^{-5}
M8	420 (720; 240)	4.2×10^{-6}
M42	3900 (5400; 2900)[c]	5.9×10^{-6}
S158A	101 (324; —)	3.2×10^{-5}
W3	4600 (7300; 3200)[d]	4.3×10^{-6}
W33	10100 (19000; 6600)	7.6×10^{-6}

[a] Uncertainty given by (the S III density at +1 σ; the S III density at −1 σ).
[b] Calculated using eq. (7).
[c] At θ^1C (see Fig. 1).
[d] At position A (see Fig. 2).

a) *The Global Density Structure of* H II *Regions*

High-resolution radio maps are a useful means for studying the global density structure of H II regions. Figures 1–5 show 6 cm radio continuum maps for M42 (Martin and Gull 1976), W3 (Harris and Wynn-Williams 1976), DR 22, G29.9−0.0, and G75.84+0.4. The maps display complicated and irregular structures; however, there are a few key morphological similarities. The most apparent is that many regions show a compact component associated with diffuse emission. This type of structure has motivated the blister model of H II regions (Habing and Israel 1979). Many compact H II regions also feature a sharp edge where the radio emission drops rapidly. This has been interpreted as the ionization fronts between the H II region and a neutral cloud (Israel 1978). We must take these morphological features into account if we want to understand the [S III] emission from these nebulae.

In order to determine the density structure from a two-dimensional radio map, we must make assumptions about the depth and symmetry of the region. By assuming spherical symmetry, we can invert the radio map to determine the density structure of the region. This technique is applied to DR 22 and G75.84+0.4 (Figs. 3 and 5) because of the circular symmetry of the compact components. Although both show an asymmetric diffuse component, our IR beam size is small enough (28″) that only the diffuse emission that extends in front of or behind the compact region is measured in our S III observations. This diffuse emission will increase the value we determine for the electron density; however, we will assume that the contribution of the diffuse emission is small.

The observed intensity distribution is approximated with a spherically symmetric model by replacing each contour on the radio map with a concentric circular contour. The emission coefficient of the gas as a function of radius is then determined by an Abel-type inversion of the intensity map (see James and James 1976). This technique can be applied to the intensity distribution of any spherically symmetric, optically thin nebula. The emissivity at a given radius is related to the observed intensity distribution by

$$j(r) = -\frac{1}{\pi r}\frac{d}{dr}\int_r^R db\,\frac{bI(b)}{\sqrt{b^2 - r^2}}, \qquad (3)$$

where R is the outer radius of the cloud, $j(r)$ is the emissivity at distance r from the center of the cloud, and $I(b)$ is the intensity of a ray with impact parameter b. The electron density is then computed from the free-free emissivity

$$n_e^2(r) = 1.06 \times 10^{10} j(r) \left(\frac{\nu}{5\ \mathrm{GHz}}\right)^{0.1} \left(\frac{T_e}{7500\ \mathrm{K}}\right)^{0.35} \mathrm{cm}^{-6} . \quad (4)$$

The temperature is taken to be approximately 8000 K, and $j(r)$ is in units of Jy pc^{-1} sr^{-1}. We adopt a distance of 3.4 kpc for DR 22 (Pipher *et al.* 1984) and 5.5 kpc for G75.84+0.4 (Matthews *et al.* 1973), a total flux of 3.2 Jy for DR 22 at 10.5 GHz (Felli, Tofani, and D'Addario 1974), and a total flux of 7.8 Jy for G75.84+0.4 at 10.7 GHz (Matthews *et al.* 1973). The term $n_e(r)$ is shown for DR 22 and G75.84+0.4 in Figure 7. We immediately notice a contrast between the two regions. DR 22 shows a relatively constant electron density with radius, while G75.84+0.4 shows an almost constant density gradient from the center to the outer edge of the region. Interestingly, in the case of G75.84+0.4, the S III density is significantly larger than the radio density; while in the case of DR 22, the S III density is consistent with the radio density (Table 3). To determine whether the density gradient in G75.84+0.4 is responsible for the difference between the S III density and the radio density, we must model the [S III] emission using the density structure we have just deduced.

b) *Modeling the* S III *Emission*

The S III emission from H II regions depends on three parameters; the density structure, the distribution of S III in the nebulae, and the abundance of sulfur. We have determined the electron density structure of DR 22 and G75.84+0.4. To model the S III emission, we assume that all the hydrogen in the nebulae is ionized and all the sulfur in the S III zone of the nebula is in the form of S III (i.e., S II or S IV zones do not overlap with the S III zone). Adding the assumption of spherical symmetry, the S III distribution can be described by two parameters, the inner and outer radii of the S III zone.

Observations of the S III to S IV abundance ratio can be used to constrain the inner radius of the S III zone. The ratio of the abundances of these ions is proportional to the relative volumes of the S III and S IV zones. The relative abundances can be determined from the comparison of the [S III] 18.71 μm line and [S IV] 10.5 μm line strengths. The S IV line has been observed for several of our sources (see Herter *et al.* 1981, 1982*a*; Pipher *et al.* 1984). The S III to S IV abundance ratio is given by

$$\frac{n_{\mathrm{S\,III}}}{n_{\mathrm{S\,IV}}} = \frac{F_{\mathrm{S\,III}}}{F_{\mathrm{S\,IV}}} \frac{j_{\mathrm{S\,IV}}/n_e n_i}{j_{\mathrm{S\,III}}/n_e n_i} e^{-0.23\tau_{9.7}} , \quad (5)$$

where $F_{\mathrm{S\,III}}$ and $F_{\mathrm{S\,IV}}$ are the [S III] and [S IV] line fluxes and $j_{\mathrm{S\,III}}/n_e n_i$ and $j_{\mathrm{S\,IV}}/n_e n_i$ are the [S III] and [S IV] emission coefficients. We have adopted $\tau_{10.5} = 0.85\tau_{9.7}$ and $\tau_{18.71} = 0.62\tau_{9.7}$ from Herter *et al.* (1982*a*), where $\tau_{9.7}$ is again the optical depth at 9.7 μm. Using the most recent S III flux measurements, and the S III density as the representative density of the S III zone and S IV zone, we find that S III is far more abundant than S IV in all the observed regions. G75.84+0.4 shows a high S III to S IV abundance, indicating that the S III zone is roughly 46 times the volume of the S IV zone. A lower limit for the S III to S IV abundance in DR 22 indicates that the S III zone has a volume at least 35 times the volume of the S IV zone. The S II to S III abundance ratio is needed to competely constrain the S III distribution; however, since S II cannot be detected in obscured regions, this ratio cannot be determined for either G75.84+0.4 or DR 22.

We are left with two unconstrained parameters: the outer radius of the S III zone and the abundance of elemental sulfur. If the density structure derived from the radio maps is accurate, matching the predicted 18.7 μm line flux and the 33.5 μm to 18.7 μm line ratio to the observed flux and line ratio will determine the outer S III zone radius and the sulfur abundance. A comparison of the models to observations of G75.84+0.4 and DR 22 is given in Table 4. In this table, we give the predicted [S III] 33.5 μm/18.7 μm line ratio for different values of the outer radius of the S III, $R_{\mathrm{S\,III}}$. For any given $R_{\mathrm{S\,III}}$, the elemental sulfur abundance is then calculated from the observed 18.71 μm flux. The observed line ratio for

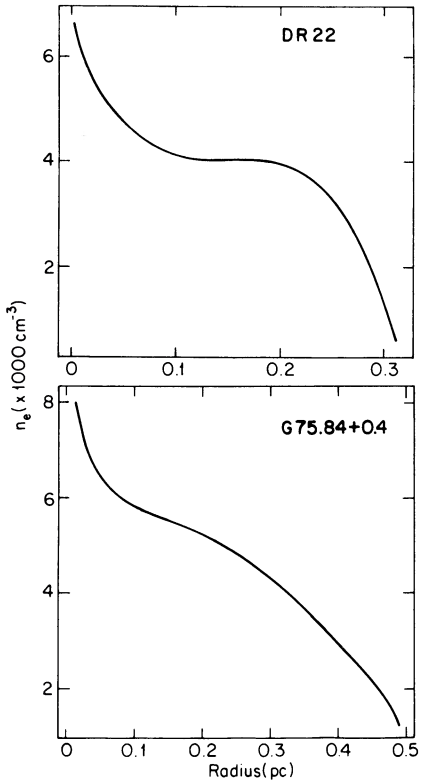

FIG. 7.—Electron density vs. radius for DR 22 and G75.84+0.4. These densities were determined by inverting the radio maps in Figs. 2 and 5 as described in text.

TABLE 4

RESULTS FROM H II REGION MODELS

$R_{\mathrm{S\,III}}/R_{\mathrm{H\,II}}$	F_{33}/F_{18}	S/H
DR 22		
0.78.....	0.35	3.5×10^{-6}
0.52.....	0.34	1.1×10^{-5}
0.47.....	0.34	1.5×10^{-5}
G75.84+0.4		
0.80.....	0.33	3.0×10^{-6}
0.54.....	0.29	7.3×10^{-6}
0.38.....	0.27	1.9×10^{-5}

G75.84+0.4 constrains $R_{S\,III}$ to be less than one-half $R_{H\,II}$, which is consistent with a sulfur abundance close to the solar abundance, S/H = 1.6×10^{-5}. For DR 22, $R_{S\,III}$ is not constrained by the observed line ratio. However, as in the case of G75.84+0.4, the abundance of sulfur approaches the solar abundance when $R_{S\,III}$ is one-half $R_{H\,III}$. We must then conclude that sulfur is underabundant in DR 22 if $R_{S\,III}$ is greater than one-half $R_{H\,II}$; however, we cannot use the sulfur abundance to constrain $R_{S\,III}$. The abundance of sulfur is known to vary with position in the galaxy; the observed sulfur abundance gradient in the galaxy indicates it is likely that sulfur will be underabundant outside the solar circle (see Pipher *et al.* 1984; Shaver *et al.* 1983).

We conclude this section with a comparison of the [S III] and rms densities for the remaining sources. Since these nebulae show a more complicated structure, a less rigorous approach must be used in modeling these regions.

G29.9−0.0.—The radio map of G29.9−0.0 shows a sharply peaked compact region surrounded by a diffuse envelope (Fig. 3). In contrast to G75.84+0.4, all of G29.9−0.0 is included in the beam of our [S III] observations. Thus, we expect that the [S III] emission could be significantly affected by the large diffuse component. Consider a simple two-component model of this source consisting of a diffuse component and a compact component. For simplicity, both components are characterized by a single density, n_d and n_c for the diffuse and compact components, respectively. Assuming that all the sulfur in the nebula is in the form of S III, the [S III] line ratio is then given by

$$\frac{F_{33}}{F_{18}} = \frac{V_d n_d^2 (j_{33}/n_i n_e) + V_c n_c^2 (j_{33}/n_i n_e)}{V_d n_d^2 (j_{18}/n_i n_e) + V_c n_c^2 (j_{18}/n_i n_e)}, \quad (6)$$

where V_d and V_c are the volumes of the diffuse and compact components, respectively. The emissivities are evaluated at the appropriate density for each component. For simplicity, we give the region a spherical symmetry by replacing the contours seen in Figure 4 with concentric, circular contours of equivalent area. We deconvolve the nebula into a compact sphere with an outer radius equal to the radius of the 50% contour, 4″ in diameter, and a diffuse shell surrounding the compact component with an outer radius equal to the radius of the 10% contour, 15″ in diameter.

Assuming that the nebula is at the near distance of 7.3 kpc and given at total radio flux of 2.9 Jy at 10.5 GHz (Felli, Tofani, and D'Addario 1974), we use equation (1) to determine that n_d is 4500 cm^{-3} and n_c is 8800 cm^{-3}. The ratio of $n_d^2 V_d$ to $n_c^2 V_c$ is 13.5. The line ratio we determine from equation (6) is 0.32, corresponding to a density of 4500 cm^{-3}. The observed line ratio is 0.20 ± 0.04, giving a density of 10,000 cm^{-3} (15,800 cm^{-3}, 7100 cm^{-3}). This shows that the S III zone cannot extend throughout the nebula, otherwise the diffuse component would dominate the S III emission due to its large volume. Like G75.84+0.4, if global density structure is to account for the measured S III density in G29.9−0.0 we require the S III zone to be confined to the compact core of the H II region.

W33.—The same approach can be used to calculate the S III emission from W33. Using the radio map and fluxes of Haschick and Ho (1983) and adopting a distance of 4 kpc, we calculate a density of 7800 cm^{-3} for the compact component and a density of 3500 cm^{-3} for the diffuse component. From this, the line ratio is determined to be 0.37, corresponding to a density of 3600 cm^{-3}. The observed line ratio is 0.20 ± 0.05, corresponding to a density of 10,000 cm^{-3} (19,000 cm^{-3}, 6600 cm^{-3}). As in the case of G29.9−0.0 and G75.84+0.4, the lower density component should dominate the [S III] emission in W33; however, since the compact component has a density consistent with the S III density, the model derived S III density can be biased to the observed S III density by reducing the size of the S III zone to the size of the compact core.

S158.—Unlike our previous sources, S158 is distinguished by its unusually low value of the S III density. A 6 cm map of S158 shows a diffuse shell 3′.6 in diameter associated with a small compact region 9″ in diameter (see Israel 1977). The 30″ beam of the S III observations was centered on the infrared source IRS 5, which is coincident with the compact region. The low density given by the S III line ratio, less than 320 cm^{-3}, implies that the S III emission is dominated by the diffuse region. Thus, in contrast to G29.9−0.0, G75.84+0.4, and W33, the S III zone in S158 extends throughout the diffuse regions of the nebula. Furthermore, the low S III density excludes the possibility of clumping in the nebula.

M8.—Like S158, M8 exhibits an unusually low S III density of 432 (724, 241) cm^{-3}. The radio density for the compact component of the region is 4400 cm^{-3} (Woodward *et al.* 1986). One possible reason for the difference between the radio density and the S III density is that the optical depth at 9.7 μm may be significant for some parts of the ionized nebula. Optical maps show that parts of the nebula are obscured and that the extinction varies greatly across the nebulae. If extinction is responsible, then $\tau_{9.7}$ must be close to 3. This is an enormously high extinction for an optically visible and nearby (1.5 kpc) region. We find it much more likely that the [S III] lines are dominated by emission from the low-density regions of the nebula. Thus, as in S158, the S III distribution may extend throughout a large diffuse component.

M42 and W3.—In the regions M42 and W3, the [S III] emission was measured for several beam positions. The locations of the beam positions are shown in the radio map of this region (Figs. 1 and 2). Tables 5 and 6 give the S III density for these positions in M42 and W3, respectively. The electron densities show a global density gradient in W3, varying from a peak of 4600 cm^{-3} in the northwestern end of the nebula to a low of 2100 cm^{-3} in the southwestern end. The density gradients correlate well with the intensity gradients seen in radio continuum maps of these regions. For the more compact region of W3 (the area within the 50% contour of Fig. 2), the rms electron density is 4400 cm^{-3}, in good agreement with the [S III] density. In M42, the S III emission was observed at θ^1C (Table 3). The density derived for this region is 4200 cm^{-3}, also in good agreement with the rms electron density of 3400 cm^{-3}. For three positions in the outer portion of the nebula the density is lower (see Fig. 1), showing again that the density peaks in the region of highest radio emission. Both M42 and W3 will be discussed in more detail in the following section.

c) *The Ionization Structure of* H II *Regions*

We have created a consistent picture in which the S III density is biased by global density gradients. In this scenario, the observed S III density is dependent on the distribution of S III within a changing density distribution. Low values of the density in a nebula result from the S III zone extending into a large diffuse envelope surrounding the compact components of the H II regions. High values of the density result when the S III zone does not extend out of the inner, more compact regions of the nebula. For G29.9−0.0, G75.84+0.4, and W33, which

TABLE 5

S III MAP OF M42

Position (α, δ)[a]	18.7 μm Flux[b]	33.5 μm Flux[b]	Density (cm^{-3})[c]	S III/H
A: (0″, 0″)	36 ± 4	<9	>6000	$>4.2 \times 10^{-6}$
C: (0, −50)	13 ± 2	<7	>1900	$>2.1 \times 10^{-6}$
D: (0, −75)	24 ± 3	19 ± 2	1000 (1400; 800)	$2.0 \pm 0.2 \times 10^{-6}$
E: (0, −100)	37 ± 4	28 ± 4	1100 (1600; 800)	$2.9 \pm 0.3 \times 10^{-6}$
F: (0, −125)	19 ± 2	14 ± 2	1200 (1600; 900)	$2.7 \pm 0.3 \times 10^{-6}$

[a] All positions relative to the 5 GHz radio peak at $\alpha_{1950} = 5^h32^m47^s.6$, $\delta_{1950} = -5°25'17''$ (Martin and Gull 1976).

[b] S III line flux in units of 10^{-18} W cm^{-2}.

[c] Uncertainty given by (the S III density at $+1\,\sigma$; the S III density at $-1\,\sigma$).

have high values of the S III density relative to the radio density, this imples that the S III zone occupies a small fraction of the volume of the nebula. We must now consider whether this picture is consistent with current observations and modeling of the ionization structure of H II regions.

For two regions, W3 and M42, the ionization structure can be observationally examined. For W3, we can examine the ionization structure by measuring the spatial extent of S III in the nebula. In M42, we can determine the ionic structure by comparing S II, S III, and S IV abundances at a given location in the nebula. The S III abundance is estimated as (see Herter *et al.* 1981):

$$\frac{n_{\rm S\,III}}{n_{\rm H}} = \frac{F_{\rm S\,III} D^2}{n_e^2 V (j/n_e n_i)}, \tag{7}$$

where $F_{\rm S\,III}$ is the S III line flux, $n_e^2 V/D^2$ is determined using the radio flux density in the S III beam, and $j/n_e n_i$ is the emission coefficient of S III per ion per electron. The term $j/n_e n_i$ is independent of the electron density for low densities ($n_e < 1000$ cm^{-3}) and varies as $1/n_e$ for higher densities. In an inhomogeneous nebula, the S III density provides the best estimate of electron density, since it reflects the density of the gas from which the S III emission originates. Using the 18.71 μm line flux for $F_{\rm S\,III}$, the abundance was calculated for M42 and each position in W3 (Tables 3 and 5).

The S III abundances for W3 (Table 6) show that S III is abundant throughout the nebula. Thus, on the basis of its spatial extent we argue that the S III zone dominates the ionic structure of W3. Note that the S III abundance in W3 does exhibit a fair amount of variation. This variation may be due to differential extinction (see Hackwell *et al.* 1978), the existence of high-density components which are not well represented in the [S III] emission, or variations in the ionic structure.

In M42, measurements taken 20″ north of θ^1C give an S III abundance of 7.7×10^{-6}. Using the S IV line flux for the same position (Herter *et al.* 1982*a*), we find a low S IV abundance for the same position, 1.1×10^{-6}. The S III abundance determined at the θ^1C position is 5.9×10^{-6} (Table 3). Since θ^1C is the exciting star, the difference between these positions is probably due to an increased S IV abundance in the θ^1C position. This implies that the S IV abundance at θ^1C is 2.9×10^{-6}. The fluxes of the S II optical lines have been measured for a similar position by Peimbert and Torres-Peimbert (1977). Using a 5″.2 × 77″.6 slit at a position 45″ N of θ^1C, the S II abundance is measured as 4.1×10^{-7}. Summing the S II, S III, and S IV abundance for this region, we get 9.2×10^{-6}, showing that sulfur abundance in M42 is 58% of the solar abundance. The comparison of the S III abundance to the S II and S IV abundances shows that S III is the dominant ion and that the S III zone must extend throughout most of the nebula. Note that for positions C, D, and E, the S III abundances are substantially lower than the θ^1C abundance (Table 5), suggesting that S II is the dominant ion in the southeastern corner of the nebula.

The small S III zone predicted for G29.9−0.0, G75.84+0.4, and W33 is not apparent in M42 or W3; however, neither M42 or W3 exhibit the high values of the S III density observed in the former three regions. Since we have measured the ionization structure in only two nebulae, we must depend on modeling to examine a wider range of H II regions.

For a wide range of parameters, models of the ionization structure predict that the S III abundance dominates the S II abundance. For stellar temperatures ranging from 31,000 to 40,000 K and uniform densities ranging from 100 to 10,000

TABLE 6

S III MAP OF W3

Position (α, δ)[a]	18.7 μm Flux[b]	33.5 μm Flux[b]	Density (cm^{-3})[c]	S III/H
A: (−6.25″, 6.25″)	43.6 ± 5.8	30.4 ± 4.9	4600 (7300; 3200)	$4.3 \pm 1.1 \times 10^{-6}$
B: (6.25, 6.25)	41.9 ± 1.7	34.5 ± 2.0	3500 (4500; 2900)	$3.4 \pm 0.8 \times 10^{-6}$
C: (18.75, 6.25)	30.4 ± 1.3	27.7 ± 3.1	3000 (4100; 2300)	$4.1 \pm 0.9 \times 10^{-6}$
D: (−6.25, −6.25)	52.7 ± 4.5	42.6 ± 2.0	3600 (4800; 2900)	$6.3 \pm 1.4 \times 10^{-6}$
E: (6.25, −6.25)	28.8 ± 2.4	36.5 ± 2.0	1800 (2400; 1400)	$2.8 \pm 0.6 \times 10^{-6}$
F: (−6.25, −18.75)	29.9 ± 1.1	37.4 ± 1.8	1800 (2300; 1500)	$6.7 \pm 1.4 \times 10^{-6}$
G: (6.25, −18.75)	16.5 ± 1.0	19.3 ± 2.9	2000 (2900; 1500)	$3.5 \pm 0.8 \times 10^{-6}$

[a] All coordinates are relative to the position of W3 IRS 2 at $\alpha_{1950} = 2^h21^m56^s.97$, $\delta_{1950} = 61°52'40''.7$ (Wynn-Williams, Becklin, and Neugebauer 1974).

[b] S III line flux in units of 10^{-18} W cm^{-2}.

[c] Density derived using $\tau_{9.7} = 1.9 \pm 0.3$. Uncertainty given by (the S III density at $+1\,\sigma$; the S III density at $-1\,\sigma$).

cm^{-3}, Rubin (1985) has shown that the S II abundance is never greater than 20% of the S III abundance. These results imply that the outer radius of the S III zone is comparable to the outer radius of the H II zone. Other modeling has included an exponential density gradient along one dimension to simulate the density structure of a blister region. In such a case, Rubin (1984) finds that for an exciting star of 35,000 K, S III again is the dominant ion in the nebula.

In conclusion, if the global density gradients result in the high [S III] densities observed in G29.9, G75.84, and W33, the S II to S III ratio must be in excess of that predicted by current H II region models. Previous observations have also suggested that current models do not adequately account for the lower ionization states in H II regions. Mid-infrared forbidden-line measurements of compact H II regions give an S III to S IV and Ar II to Ar III ratio in excess of those predicted by models (see Herter, Helfer, and Pipher 1983). These discrepancies may be the result of the failure of stellar models of O and B stars or inaccurate descriptions of the absorption properties of dust grains in the far-UV (below 912 Å) or both. Because of these effects, we cannot rule out the possibility that the S III zone is confined to the dense inner regions of the nebula, and that the global density structure can account for the observed [S III] densities.

V. IONIZED CLUMPS AND NEUTRAL CONDENSATIONS

Although the global density picture gives a plausible explanation for the high values of the S III density found in G29.9−0.0, G75.84+0.4, and W33, it is not unique. An alternative explanation is that the high densities determined from the [S III] observations may be the result of small-scale density enhancements (clumping).

As we mentioned previously, optical measurements of the [S II] and [O II] line ratios have given electron densities much higher than rms densities in some nebulae. These observations have motivated the model that the ionized gas in H II regions is clumped. This model is further supported by the structure shown in optical images of nebulae. It is therefore natural to assume that high S III densities observed in some nebulae may also be the result of clumping. Although extensive clumping is not observed in high-resolution radio observations ($<1''$) of compact H II regions, it is easy to imagine how these clumps avoid detection. Even if they are large enough to be resolved in radio maps, the superposition of many clumps will be indistinguishable from a smooth distribution of gas.

One caveat to the clumping model is that it is not understood how high-density, fully ionized clumps can exist in an H II region. Since the temperature of the gas increases with density (see Osterbrock 1974), clumps of ionized gas cannot be in pressure equilibrium with a surrounding diffuse component and will have a lifetime much shorter than the age of the H II region. For ionized clumps to exist, an unknown mechanism must either preserve clumps or continuously create clumps. For this reason, we find the existence of optically thin, fully ionized clumping unlikely.

Dense clumps of ionized gas have been resolved in high-resolution radio continuum maps of M42 (see Garay, Moran, and Reid 1987). These maps show 13 clumps within 30″ of θ^1C. They have densities greater than 10^5 cm^{-3} and are less than 10^{-3} pc in diameter. Since the lifetime of fully ionized clumps is short compared to the age of the nebula, Garay, Moran, and Reid explain these clumps as high-density, ionized gas flowing off neutral condensations (see Dyson 1968). Unlike completely ionized clumps, theoretical models show that these condensations can have lifetimes of 10^5 yr and may be remnants of the original star-forming cloud (see Tenorio-Tagle 1977).

The high-density component observed by Garay, Moran, and Reid in M42 contains only a small percentage of the mass of the nebula. For clumping to account for the high values of the S III density observed in G29.9−0.0, G75.84+0.4, and W33, the high-density component must contain most of the mass of the nebulae. As argued from lifetime considerations, the clumps must be dense, ionized envelopes surrounding neutral condensations. Surrounding such a condensation is an inverse H II region. The low-excitation ions (S II and O II) are found in the higher density gas close to the condensations, and the high-excitation ions (S III) are found further from the condensation in a lower density gas. Since the [S III] emission is biased toward low-density regions, it is difficult to picture how neutral condensations can significantly affect the S III density without filling much of the ionized nebula with globules of neutral gas. In contrast, the [S II] and [O II] emission is biased toward high-density regions, and optical line ratios may be biased by neutral condensations. This effect may have been observed in the high electron densities measured in M42 using [S II] and [O II] observations (see Osterbrock and Flathers 1959; Danks and Meaborn 1971; Menon 1961).

Although it is unlikely that small-scale structure is directly responsible for the high values of the S III density observed in G29.9−0.0, G75.84+0.4, and W33, neutral condensations could alter the ionization structure by shadowing the outer regions of the nebulae from the direct illumination of the exciting star. In these shadows, the diffuse radiation field would dominate, allowing only the existence of low-excitation ions such as S II. Thus, neutral condensations would reduce the volume of the S III zone, biasing the observed value of the S III density. One could further speculate that as the H II region evolved, the condensations would evaporate and the S III zone would expand into the nebula; in this case, regions such as S158 and M8 would be more evolved than G29.9−0.0, G75.84+0.4, and W33. In conclusion, we suggest that it is more likely that small-scale structure can alter the S III density by altering the ionization structure rather than by directly increasing the local gas density.

VI. ABUNDANCE ESTIMATES IN INHOMOGENEOUS NEBULAE

One motivation for gaining a detailed understanding of the density and ionic structure of compact H II regions is to more accurately predict elemental abundances. The abundances of S III relative to H II in an ionized nebula can be estimated using equation (7), as we have already done for M42 and W3 (Tables 3, 5, and 6). Table 3 gives the S III abundance for the remainder of our sources.

The ratio of the sulfur to hydrogen abundances can be determined by summing the S II, the S III, and the S IV abundances (see Herter *et al.* 1981). The major uncertainty is the S II abundance, which has been observed only for M42. For M42 and W3, we have shown that the S III zone dominates the nebula. For these regions, we believe that the S III abundances shown in Tables 3, 5, and 6 are a good estimate of the elemental sulfur abundance. In the case that S III is not the dominant ion, the S III abundance is a lower limit of the sulfur abundance. This implies that the sulfur abundance of G29.9−0.0, whose S III abundance is 3.5×10^{-5}, is at least 2.2 times the solar value.

If we assume that the global density gradient picture is correct, the S III zones of these nebulae fill a small fraction of

the volume of the H II region. To determine the sulfur abundance, we must consider only the region within the S III zone, replacing $n_e^2 V$ integrated over the whole H II region with $n_e^2 V$ integrated over the S III zone. For G75.84+0.4, this is consistent with an abundance close to the solar value (Table 4). If we assume that the S III zones for G29.9−0.0 and W33 are confined to the compact cores observed in these regions (see § IV*b*), then the sulfur abundance for W33 is 2.8×10^{-5}, 1.8 times the solar abundance, and the sulfur abundance for G29.9−0.0 is 5.1×10^{-5}, 3.2 times the solar abundance. These factors are not unexpected for regions in the 5 kpc star formation ring, which shows other evidence for enhanced metal abundance (see Lester *et al.* 1987). Finally, if the radius of the S III zone in DR 22 is half the radius of the H II zone, the sulfur abundance for the region approaches the solar value. Thus, the sulfur abundances produced using the global density picture are reasonable.

VII. CONCLUSIONS

We have examined the density structure of compact H II regions using the [S III] 33.5 and 18.7 μm fine-structure lines and 6 cm radio continuum maps. The densities derived from the [S III] fine-structure lines are listed in Table 3. Since the observed nebulae are inhomogeneous, the observed [S III] emission was compared to the [S III] emission predicted from models derived from the radio maps. Comparing the radio and infrared data we find the following:

1. The density derived from the [S III] emission is consistent with the density derived from the radio for DR 22, M42, and W3. We also find that for the latter two regions, the S III zone extends throughout most of the H II zone. For DR 22, our data do not constrain the size of the S III zone. In S158 and M8, the low derived densities imply that the [S III] emission is dominated by a diffuse component of the nebula.

2. The [S III] densities in G29.9−0.0, G75.84+0.4, and W33 are much higher than the radio densities. We have considered two explanations of this difference. First, the S III zone may be restricted to the small, compact centers of the H II regions biasing the [S III] density. This implies S III zones less than half the radius of the H II zones. This is in contrast to current models of the ionization structure, which indicate that the S III zone should extend throughout most of the nebula.

An alternative explanation is that the ionized gas in the nebulae is clumped. The main difficulty in this explanation is that the clumps would not be in pressure equilibrium with the surrounding gas, and the lifetime of the clumps would be small compared to the age of the nebula. If fully ionized clumps exist in nebulae, an unknown mechanism must preserve or regenerate the clumps.

3. Comparison of the S II, S III, and S IV abundances in M42 show that the S III zone extends throughout most of the nebula and is the dominant ionic component of the nebula. Thus, the [S III] derived densities, 6000 to 1000 cm^{-3}, are representative of much of the region. These lines are insensitive to a high-density component, such as the clumps of ionized gas found near θ^1C in high-resolution radio maps of M42 (Garay, Moran, and Reid 1987). Garay, Moran, and Reid (1987) explain the clumps as high-density ionized gas flowing off neutral condensations. Since neutral condensations can exist as long as 10^5 yr, they may be remnants of the molecular cloud from which the H II region formed. It is possible that the [S II] and [O II] line emission in M42 may be biased by clumps such as these, resulting in the high densities some observers have measured in the nebula. These neutral condensations probably exist in other nebulae, and we suggest that although these condensations cannot directly influence the S III density, they may shadow the outer regions of nebulae, resulting in small S III zones in G29.9−0.0, G75.84+0.4, and W33.

Current observations cannot distinguish between the global density gradient and clumping pictures. A key to distinguishing the two pictures is understanding the S III distribution in the nebula. Unfortunately, the infrared fine-structure lines at 33 and 18 μm cannot yet be measured with sufficient spatial resolution to map most H II regions. High-resolution observations will give direct information on the ionic and density structure of compact H II regions.

We thank the staff of the Kuiper Airborne Observatory for their excellent support that made these observations possible. This work was funded by NASA-Ames Grant NAG 2-207.

REFERENCES

Danks, A. C., and Meaborn, J. 1971, *Ap. Space Sci.*, **11**, 398.
Downes, D., Goss, W. M., Schwartz, U. J., and Wouterloot, J. G. A. 1978, *Astr. Ap. Suppl.*, **35**, 1.
Dyck, H. M., and Simon, T. 1977, *Ap. J.*, **211**, 421.
Dyson, J. E. 1968, *Ap. Space Sci.*, **1**, 388.
Felli, M., Tofani, G., and D'Addario, L. R. 1974, *Astr. Ap.*, **31**, 431.
Garay, G., Moran, J. M., and Reid, M. J. 1987, *Ap. J.*, **314**, 535.
Habing, H. J., and Israel, F. P. 1979, *Ann. Rev. Astr. Ap.*, **17**, 345.
Hackwell, J. A., Gehrz, R. D., Smith, J. R., and Briotta, D. A. 1978, *Ap. J.*, **221**, 797.
Harris, S., and Wynn-Williams, C. G. 1976, *M.N.R.A.S.*, **174**, 649.
Haschick, A. D., and Ho, P. T. P. 1983, *Ap. J.*, **267**, 638.
Herter, T., Briotta, D. A., Jr., Gull, G. E., Shure, M. A., and Houck, J. R. 1982*b*, *Ap. J.*, **262**, 164.
Herter, T., Helfer, H. L., and Pipher, J. L. 1983, *Astr. Ap. Suppl.*, **51**, 195.
Herter, T., Helfer, H. L., Pipher, J. L., Briotta, D. A., Jr., Forrest, W. J., Houck, J. R., Rudy, R. J., and Willner, S. P. 1982*a*, *Ap. J.*, **262**, 153.
Herter, T., *et al.* 1981, *Ap. J.*, **250**, 186.
Houck, J. R., and Gull, G. E. 1982, *Proc. SPIE*, **363**, 46.
Israel, F. P. 1976, *Astr. Ap.*, **48**, 193.
———. 1977, *Astr. Ap.*, **59**, 27.
———. 1978, *Astr. Ap.*, **70**, 769.
Israel, F. P., Habing, M. J., and de Jong, T. 1973, *Astr. Ap.*, **27**, 143.
James, G., and James, R. C. 1976, *Mathematics Dictionary* (New York: Reinhold).
Klein, R. I., Sandford, M. T., II, and Whitaker, R. W. 1983, *Ap. J. (Letters)*, **271**, 69.
Lester, D. F., Dinerstein, H. L., Werner, M. W., Watson, D. M., Genzel, R., and Storey, J. W. V. 1987, *Ap. J.*, **320**, 573.
Martin, A. H. M., and Gull, S. F. 1976, *M.N.R.A.S.*, **175**, 235.
Matthews, H. E., Goss, W. M., Winnberg, A., and Habing, H. J. 1973, *Astr. Ap.*, **29**, 309.
Melnick, G., Gull, G. E., and Harwit, M. 1979, *Ap. J. (Letters)*, **227**, L35.
Mendoza, C. 1983, in *IAU Symposium 103, Planetary Nebulae*, ed. D. R. Flower (Dordrecht: Reidel), p. 143.
Menon, T. K. 1961, *Pub. N.R.A.O.*, **1**, No. 1.
Osterbrock, D. E. 1974, *Astrophysics of Gaseous Nebulae* (San Francisco: Greeman).
Osterbrock, D. E., and Flathers, E. 1959, *Ap. J.*, **129**, 26.
Peimbert, M., and Torres-Peimbert, S. 1977, *M.N.R.A.S.*, **179**, 217.
Pipher, J. L., Grasdalen, G. L., and Soifer, B. T. 1974, *Ap. J.*, **193**, 283.
Pipher, J. L., Helfer, H. L., Herter, T., Briotta, D. A., Jr., Houck, J. R., Willner, S. P., and Jones, R. 1984, *Ap. J.*, **285**, 174.
Rubin, R. H. 1984, *Ap. J.*, **287**, 653.
———. 1985, *Ap. J. Suppl.*, **57**, 349.
Rubin, R. H., Simpson, J. P., Erickson, E. F., and Haas, M. R. 1988, *Ap. J.*, **327**, 377.
Sandford, M. T., II, Whitaker, R. W., and Klein, R. I. 1984, *Ap. J.*, **282**, 178.
Shaver, P. A., McGee, R. X., Newton, L. M., Danks, A. C., and Pottash, S. R. 1983, *M.N.R.A.S.*, **204**, 53.
Tenorio-Tagle, G. 1977, *Astr. Ap.*, **54**, 517.
Woodward, C. E., Helfer, H. L., and Pipher, J. L. 1985, *Ap. J.*, **147**, 84.
Woodward, C. E., *et al.* 1986, *A.J.*, **91**, 870.
Wynn-Williams, C. G., Becklin, E. E., and Neugebauer, G. 1974, *Ap. J.*, **187**, 473.

G. E. Gull, T. Herter, J. R. Houck, and S. T. Megeath: Center for Radiophysics and Space Research, Space Sciences Building, Ithaca, NY 14853